·Article·
Advances in Polar Science
doi: 10.3724/SP.J.1085.2013.00060
March 2013 Vol. 24 No. 1: 60-68

Optical and SuperDARN radar observations of duskside shock aurora over Zhongshan Station

LIU Jianjun[1*], HU Hongqiao[1], HAN Desheng[1], LIU Yonghua[1], ZHANG Qinghe[1] & Akira S Yukimatu[2]

[1] SOA Key Laboratory for Polar Science, Polar Research Institute of China, Shanghai 200136, China;
[2] National Institute of Polar Research, Tokyo 190-0014, Japan

Received 1 January 2013; accepted 7 March 2013

Abstract We present observations of a duskside shock aurora occurred on 21 April 2001 by the SuperDARN radar at Syowa Station and the all-sky camera at Zhongshan Station (ZHS) in Antarctica when the radar was operated in fast-scan mode covering the ZHS region. With the two independent data sets, we examine ionospheric plasma convection and aurora arising from a sudden impulse (SI) event associated with an interplanetary shock. During the transient shock compression, the aurora was quiescent without any optical emission at the preliminary impulse of the SI. About 7 min later, a new thin auroral arc with brighter emissions and a lifetime of ~14 min expanded westward from the region above ZHS during the main impulse of the SI. SuperDARN radar line-of-sight measurements showed periodical oscillation in the flow direction with ultra-low-frequency waves having a period of ~8 min during the shock compression. We suggest that downward field-aligned current during the preliminary impulse stage of the SI was the main driver of the first plasma flow reversal, and the subsequent new discrete auroral arc may be associated with field-aligned acceleration in the region of the main impulse related upward field-aligned currents. The ground magnetometer observations suggest that the oscillation of the ionospheric convection on the duskside was associated with field line resonance activity.

Keywords **SuperDARN radar, shock aurora, sudden impulse, flow reversal**

Citation: Liu J J, Hu H Q, Han D S, et al. Optical and SuperDARN radar observations of duskside shock aurora over Zhongshan Station. Adv Polar Sci, 2013, 24:60-68, doi: 10.3724/SP.J.1085.2013.00060

1 Introduction

Interplanetary (IP) shock and a sudden enhancement of the solar wind dynamic pressure can greatly disturb the Earth's magnetic field, triggering a sudden commencement (SC) or sudden impulse (SI) that manifests as a steplike increase in the northward component of the geomagnetic field observed by a ground magnetometer[1-2]. The magnetic field at the geosynchronous orbit is strongly compressed on the dayside when an IP shock arrives[3]. Energetic particle dynamics in the magnetosphere are also affected by IP shocks. The temporal and spatial distributions of density and temperature of energetic particles change prominently, while a strong electromagnetic ion cyclotron wave and electron whistler wave on the dayside are induced by IP shock compression[4]. The injection of energetic particles into the inner magnetosphere by IP shocks has been observed[5]. Zhang et al.[6] reported that when a sudden increase in the solar wind dynamic pressure impinges on the magnetopause, ultra-low-frequency (ULF) waves are excited in the magnetosphere, significantly enhancing the energy coupling efficiency between the solar wind and magnetosphere. It is well known that ULF waves due to field line resonance (FLR) activity play an important role in the transfer of energy into and around the magnetosphere and ultimately into the ionosphere. Furthermore, energetic particles are accelerated by the induced ULF waves[7].

Just after the SC/SI, transient auroral emissions (referred to as a "shock aurora") caused by IP shock compres-

* Corresponding author (email: liujianjun@pric.gov.cn)

sion develop on a global scale[8-12]. Satellites have observed that a shock aurora immediately brightens near local noon at the time of the shock arrival identified by the ring current index of SYM-H. The initial brightening of a shock aurora is limited to within a few hours of magnetic local time (MLT) in the dayside ionosphere, and then propagates toward both the dawnside and duskside along the auroral oval flanks at high speed (more than ~11 km·s^{-1}) and ultimately reaches the midnight sector[10-11,13]. Boudouridis et al.[14] found that a sudden compression of the magnetosphere by an IP shock led to a global enhancement of ionospheric currents in the aurora zone and an increase in auroral emissions, with poleward expansion of the auroral oval. It has also been noted that long-duration high solar-wind ram pressure increases auroral intensity in the flanks of the auroral oval and there is dawn–dusk asymmetry of the auroral luminosity[8].

In addition to the global intensification of the aurora, an increase in solar wind dynamic pressure can significantly enhance the ionospheric convection speed in the dayside ionosphere as detected by the SuperDARN radar. The enhanced convection extends to the vicinity of the expected location of the dayside convection separatrix, suggesting that the solar wind dynamic pressure strongly affects dayside reconnection as well as polar cap convection[15-16]. Recently, Liu et al.[17] examined a shock aurora event in detail using SuperDARN radar and ground-based optical auroral data. They found auroral weakening and simultaneous plasma flow reversal in the postnoon sector for a very short time immediately after the SC onset, which means that shock compression plays an important role in auroral particle precipitation and magnetospheric plasma convection. More attention needs to be given to this type of transient IP shock in terms of ground-based observations of the associated aurora and ionospheric plasma flow to reveal the evolution of the shock triggered ionospheric phenomenon in more detail. More recently, on the basis of SuperDARN King Salmon high-frequency (HF) radar observations, Hori et al.[18] reported plasma flow reversal on the duskside during a negative SI.

Although satellite observations are useful in identifying the large-scale temporal and spatial evolution of a shock aurora, high-resolution ground-based optical measurements are needed to reveal the fine structure and detailed variation of the shock aurora. From coordinated ground optical and satellite particle measurements, Egeland et al.[19] noticed that the entire sky brightened quickly and that auroral particle precipitation was greatly enhanced during an SC event on the dawnside. Sandholt et al.[20] reported that the enhancement of the solar wind dynamic pressure leads to an equatorward movement of the intensified cusp aurora and enhanced ionospheric convection. Using simultaneous ground and satellite optical observations, Motoba et al.[12] analyzed a shock aurora event in the postnoon sector in the Southern Hemisphere and found that the transient auroral brightening on the dayside can be divided into two processes. The initial process corresponds to a diffuse aurora detected at 557.7 nm, and the subsequent process corresponds to a new discrete auroral form detected at both 557.7 and 630.0 nm. Using ground-based optical instrumentation at Ny-Ålesund in Svalbard, Zhou et al.[21] studied a shock aurora event near local noon, and found that the auroral forms presented as a diffuse type in closed field lines. Here we report a unique shock aurora event according to coordinated duskside observations made with the SuperDARN radar and an all-sky imager at the Chinese Zhongshan Station (ZHS) in Antarctica.

2 Observations

Figure 1a–1e shows the solar wind parameters observed by the ACE spacecraft around the L1 point at (234, 41, and 10) R_E in GSM coordinates during the interval 1200–2000 UT on 21 April 2001. The first vertical dashed line indicates that an IP shock approached the Earth with clear enhancement of the solar wind dynamic pressure at 1504 UT from less than 2 nPa to over 4 nPa due to quickly increasing solar wind speed V_{sw} and proton density N_{sw}. At the same time, the B_z component of the interplanetary magnetic field (IMF) was mainly positive and oscillated near zero magnitude. The IMF B_y component was negative, and the B_x component also oscillated.

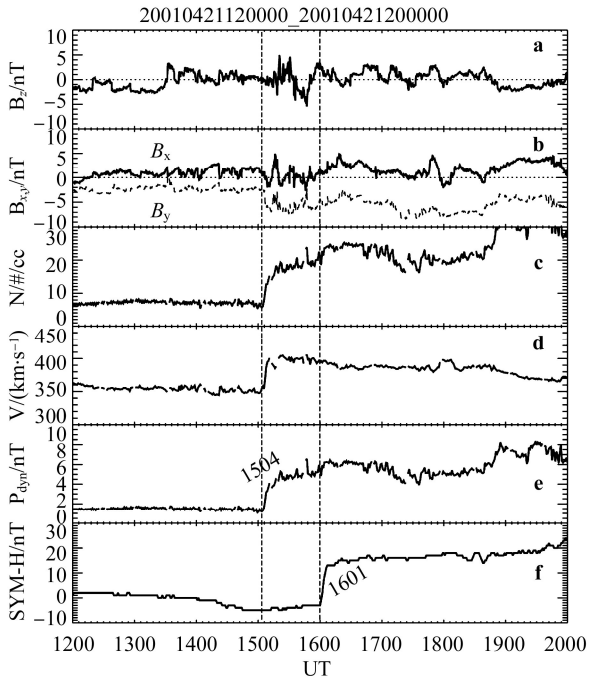

Figure 1 **a**, IMF north-south component B_z; **b**, IMF B_x and B_y in GSM coordinates; **c**, solar wind proton density N_{sw}; **d**, velocity V_{sw}; **e**, dynamic pressure P_{dyn} monitored by the ACE satellite; **f**, ring current SYM-H index on 21 April 2001. Two dashed lines indicate the shock time (1504 UT) recorded by the ACE satellite and the onset time of the SI (1601 UT) confirmed by ground observations.

About 57 min later, the IP shock arrived in Earth space and induced a sharp increase in the SYM-H index as shown by the second vertical dashed line at 1601 UT (Figure 1f).

The SYM-H index measures the mean longitudinally symmetric component of magnetic disturbances and is essentially the same as the hourly D_{st} index[22]. The SI amplitude of the SYM-H index was 17 nT.

The IP shock impinges Earth space, causing global dynamic changes in electromagnetic fields and the plasma environment. Figure 2 shows the variation in the northward component of the geomagnetic field during the interval 1550–1630 UT; i.e., throughout the IP shock passage. The magnetic field data were recorded by three magnetometers located at Jicamarca at the magnetic dip equator, Alice Springs at low latitude and Casey at high latitude (see Table 1) in the Southern Hemisphere. The time resolution of the magnetometer at Jicamarca is 1 s whereas those of the magnetometers at Alice Springs and Casey are 1 min. The more accurate SI onset time determined by the 1-s sampling data at Jicamarca was 160045 UT marked by the vertical dashed line in Figure 2, when Jicamarca was located near local noon. The stepwise change in the X-component at Alice Springs reached a peak (14 nT) before 1607 UT, and the amplitude was then almost stable around 11 nT. After the SI onset, the waveform at high latitude (Casey) showed first a negative impulse corresponding to the preliminary impulse (PI), which was referred to as the PI stage of the SI in the afternoon auroral zone[2]. The PI stage of the SI generally persists for a short period. After the PI stage of the SI, the main impulse (MI) presenting as a subsequent positive impulse began around 1608 UT. At the dayside dip equator (Jicamarca), the two impulses at high latitude are seen again.

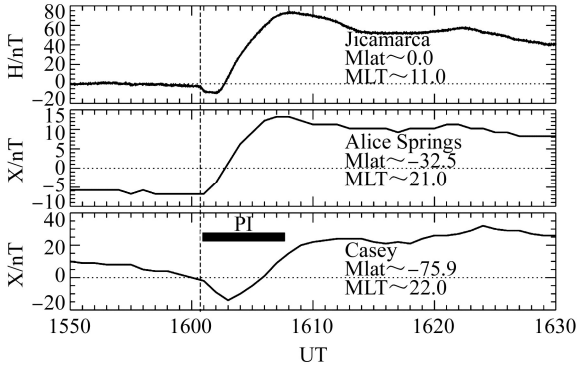

Figure 2 Geomagnetic field variations observed by magnetometers from the dip equator to the region of higher latitude. The dashed line indicates the onset time of the SI.

To reveal the fine structure of the shock aurora forms and simultaneous ionospheric plasma convection, we examined ground-based observations. During the SI event, ZHS was located on the duskside (1730 MLT). Figure 3 shows the locations and field-of-view (FOV) of the all-sky camera (ASC) at ZHS and of the Syowa East radar (69°S, 39°E in geographic coordinates, also called SENSU radar) in the Southern Hemisphere. The plot shows a polar grid of magnetic latitude (MLAT) and MLT coordinates. The auroral observation at ZHS was carried out using an advanced TV ASC fitted with a fish-eye lens. Each aurora frame had exposure time of 4 s and spatial resolution of 320×240 pixels[23]. During the present SI event, most ionospheric echoes received by SENSU radar came from the E and F regions over ZHS, providing good conjunction with the optical auroral observation; hence, the radar helped identify more detailed structures of the shock aurora on the duskside and the associated plasma flows. Assuming the discrete auroral emission height is 110 km on the duskside, the meridional coverage of the auroral frame at ZHS approximately extends from –70° to –79° in geomagnetic latitude[24]. The TV ASC at ZHS is a panchromatic imager that is sensitive to emissions at N_2^+ wavelengths of 427.8 and OI 557.7 nm[23]. It is generally considered that the 557.7 nm emission results from neutral atomic oxygen excitation directly and/or indirectly by precipitating keV electrons. Therefore, the two emissions respond primarily to the electron precipitation and are particularly useful in identifying the field-aligned current (FAC) carried by particle precipitation[25].

Table 1 Ground stations

Station name	Code	Geographic /°		Geomagnetic /°	
		Lat.	Long.	Lat.	Long.
Ny Ålesund	NAL	78.92	11.95	75.25	112.08
Longyearbyen	LYR	78.20	15.82	75.12	113.00
Hornsund	HOR	77.00	15.60	74.13	109.59
Bear Island	BJN	74.50	19.20	71.45	108.07
Muonio	MUO	68.02	25.23	64.72	105.22
Pello	PEL	66.90	24.08	63.55	104.92
Hankasalmi	HAN	62.25	26.60	58.69	104.54
Nurmijärvi	NUR	60.50	24.65	56.89	102.18
Jicamarca	JIC	-12.00	283.10	0.0	354.20
Alice Springs	ASP	-23.76	133.88	-32.50	206.92
Casey	CSY	-66.28	110.53	-75.99	184.57

Figure 4 shows the auroral sequence images taken during 1600–1638 UT in two-minute intervals. The two white arrows, marked *M.S* and *M.E* in the first frame in Figure 4, indicate the magnetic south (poleward) and east, respectively. The SI onset time identified by the geomagnetic field observation was 1601 UT, and is marked by a downward arrow in Figure 4. At this time, ZHS was located at ~1730 MLT on the duskside, as shown in Figure 3. Before the SI onset, Figure 4 shows that the ASC did not observe auroral emission over ZHS. Immediately after the SI, the whole sky over ZHS remained quiet without any notable auroral structure. This phenomenon lasted for ~7 min, which is almost equivalent to the duration of the PI stage of the SI shown in Figure 2. The first brightening of the shock aurora detected by the ASC at ZHS appeared in the northeast of the FOV at 1608 UT (shown by the white arrow in Figure 4). The auroral brightening was initially weak but

highly structured. This discrete aurora manifested as a thin arc aligned obliquely to the east-west direction. After checking the auroral sequence images at the highest time resolution of 4 s, it was found that the duskside shock aurora in discrete type moved westward (sunward) from the east edge of the FOV of the ASC at ZHS. Previous studies on shock aurora generally showed tailward propagation along the auroral oval on dusk and dawn flanks simultaneously. Until now, all work found that an antisunward propagating shock aurora was of diffuse type, and the sunward moving shock aurora thus requires further attention. At the same time, the thin arc moved poleward with increasing brightness and latitudinal width (poleward widening). About 14 min after the initial brightening of the discrete-type shock aurora, the auroral intensity slightly decreased (Figure 4).

SENSU radar, as part of the SuperDARN radar network, makes detailed observations of ionospheric plasma flow on the duskside (Figure 3). The radar sequentially scanned through all 16 beam directions over 1 min and measured the backscatter power, line-of-sight (LOS) velocity, and spectral width in 75 range gates in a fast scanning program[26]. The view of scan of SENSU radar was just over ZHS as shown by a fan-shaped FOV in Figure 3. During the SI event, the radar central beams were biased toward the duskside and their scan has the advantage of being able to detect sunward and antisunward plasma flows. Figure 5 shows time series of LOS velocity as a function of range gate measured by beams 7 and 12 of SENSU radar.

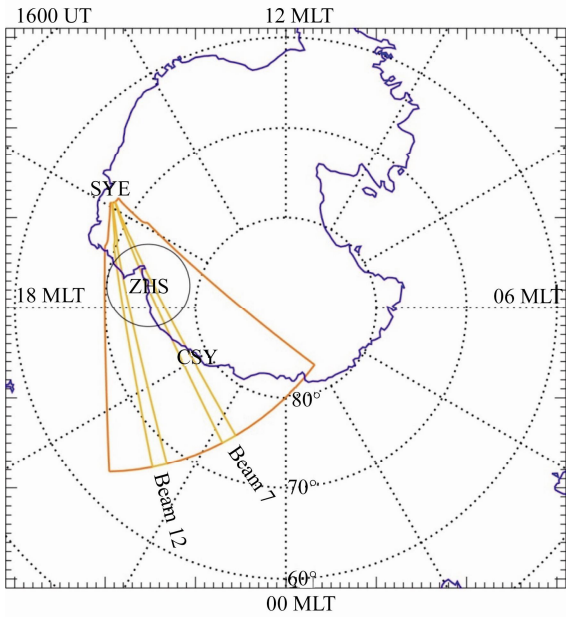

Figure 3 The FOV of the ASC at ZHS and SENSU radar in the Southern Hemisphere on an MLT/MLAT grid at 1600 UT; the Casey Station (CSY) is also shown. The concentric dotted circles represent the magnetic latitude (in 10° intervals), and the radial dotted lines represent the magnetic local time (at intervals of 2 h). Beams 7 and 12 of the SENSU radar are plotted to show the advantage of scanning sunward and antisunward plasma flow over ZHS in the duskside sector.

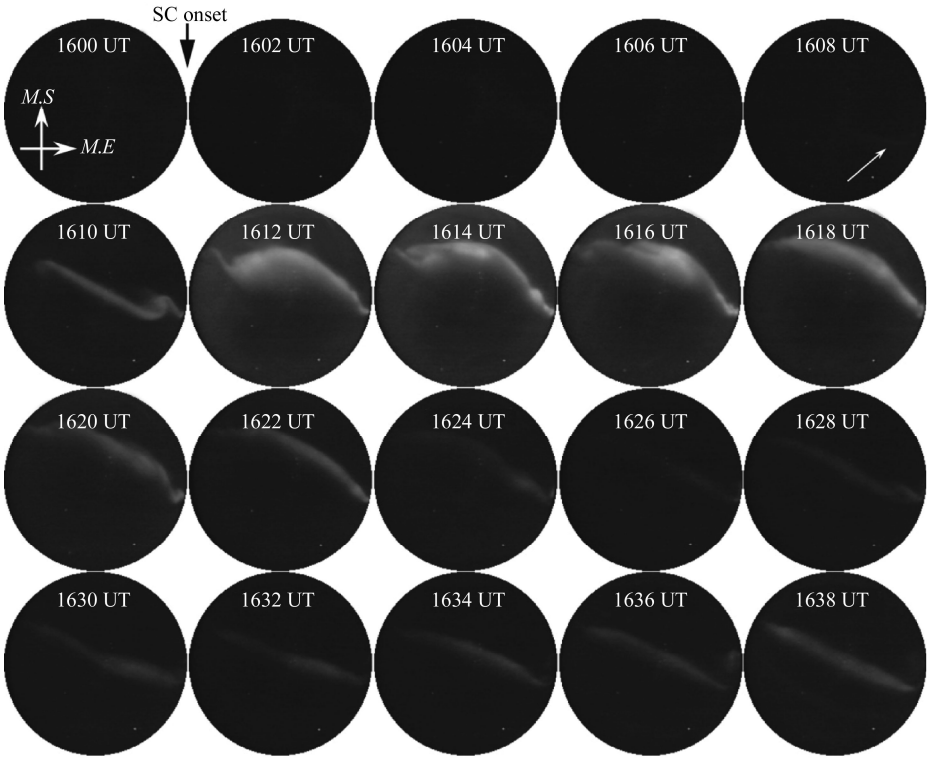

Figure 4 Auroral all-sky sequence images taken from ZHS during 1600–1638 UT. The geomagnetic south (poleward) and east directions are marked *M.S* and *M.E*, respectively.

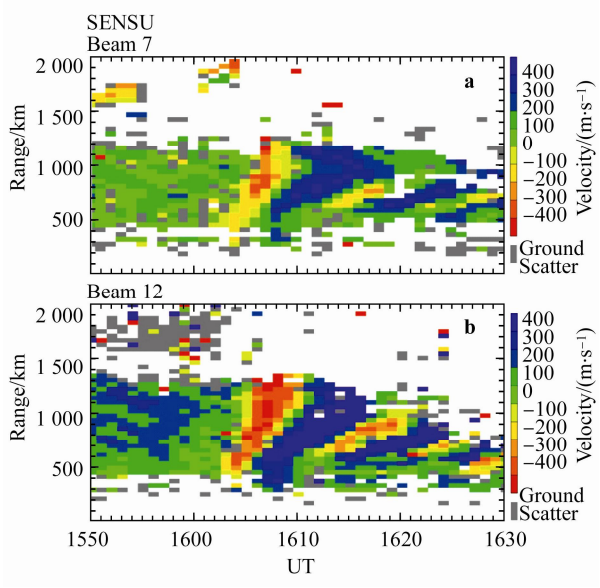

Figure 5 LOS ionospheric plasma flow scanned by beams 7 and 12. The color bar on right indicates the sunward (positive) and antisunward (negative) velocities of plasma flows.

The directions of beams 7 and 12 are shown in Figure 3. The color scale of Figure 5 shows the velocity of the plasma flow inferred from the Doppler frequency shift. Positive and negative values indicate plasma flow toward and away from the radar, respectively. Comparing with the geomagnetic field variation shown in Figure 2, we can identify the auroral activity and simultaneous ionospheric plasma convection on the duskside associated with shock compression.

From the ionospheric backscatter data for beams 7 and 12 shown in Figure 5, it is seen that the plasma flow was sunward before the SI onset with an average velocity magnitude less than 200 $m \cdot s^{-1}$ at the zenith of the ASC at ZHS. A very clear feature of the plasma flow is the sudden reversal of the flow direction, which shows that the LOS velocity reversed to antisunward immediately after the SI onset triggered by the IP shock compression. The flow reversal commenced near the radar site at a lower speed, and this reversed flow propagated to the far range gate with increasing velocity. It is noted that the preliminary flow reversal lasted for about 8 min, which is almost equivalent to the period of the PI stage of the SI shown in Figure 2. After 1607 UT, the plasma flow over ZHS returned to sunward with a higher velocity near the radar site during the MI stage of the SI. One important signature of the plasma flow reversal is the repeated periodical structure with a period of 8 min. It is noted that the backscatter data for beam 12 in the lower latitude region are similar to the signature of the beam 7 on the whole, but flow speed in the lower latitude region was evidently higher than that in the center view of the SENSU radar.

The LOS velocities in Figure 5 can be combined with the "map potential" model of ionospheric flow to derive large-scale two-dimensional velocities[27]. The LOS velocities are mapped onto a polar grid, and then fitted to an expansion of the electrostatic potential in spherical harmonics, which is stabilized by a statistical model in regions where there are no real observations. Therefore, the large-scale global plasma convection is shown for 18 min in Figure 6, and it is seen that there is complicated plasma flow in the postnoon region. During the PI stage of the SI, the ionospheric plasma convection pattern was deformed considerably, specifically in the postnoon sector with a multi-vortex flow system. A large-scale ionospheric plasma flow pattern had a typical convection twin-vortex when the SI was in the MI stage, as shown in Figure 6.

3 Discussion

We examined one shock aurora event using ground-based optical and SuperDARN radar data for the duskside in the Southern Hemisphere. The aurora observed by the ASC at ZHS during the IP shock compression was identified and its development can be divided into two steps. The first step was a quiescent period without any auroral emission immediately after the SI triggered by the IP shock; at the same time, SENSU radar observed a prompt plasma flow reversal from sunward to antisunward. About 7 min later, a new thin discrete auroral arc was observed in the northeast of the FOV of the ASC at ZHS. The thin discrete arc developing with brighter emissions expanded sunward and poleward simultaneously, and had a lifetime of ~14 min during the MI stage of the SI. There was a new signature of the plasma flow with clear periodical oscillation features having a period of 8 min after the IP shock.

It is known that precipitating particles are the main factor determining auroral brightness, and they have a close relationship with the FAC. The upgoing electrons have been identified as the carriers of the downward FACs[28-29]. Marklund et al.[30] found upgoing electrons were associated with a black aurora in the downward FAC region and indicated that a total absence of auroral emission was caused by the upgoing electrons associated with the downward FAC. Similarly, we suggest that the quiescent auroral emission over ZHS at the beginning of the SI may mostly be caused by a downward FAC that has a close relationship with the IP shock compression and the response of the magnetosphere-ionosphere coupling system.

For generation of the FACs, a well-known SI model proposed by Araki[2] predicted that downward and upward FACs are produced at the PI stage of SI in the afternoon and morning sectors, respectively. Therefore, it is reasonable to consider that the downward PI FAC suppressed the auroral particle precipitation and led to the quiescent auroral emission on the duskside, as shown in Figure 4. Such observational results for a shock aurora were reported by Liu et al.[17] according to observations made by the same auroral optical imager but for a different shock aurora event.

SuperDARN radar is a powerful tool with which to determine FACs through convection observations, and it

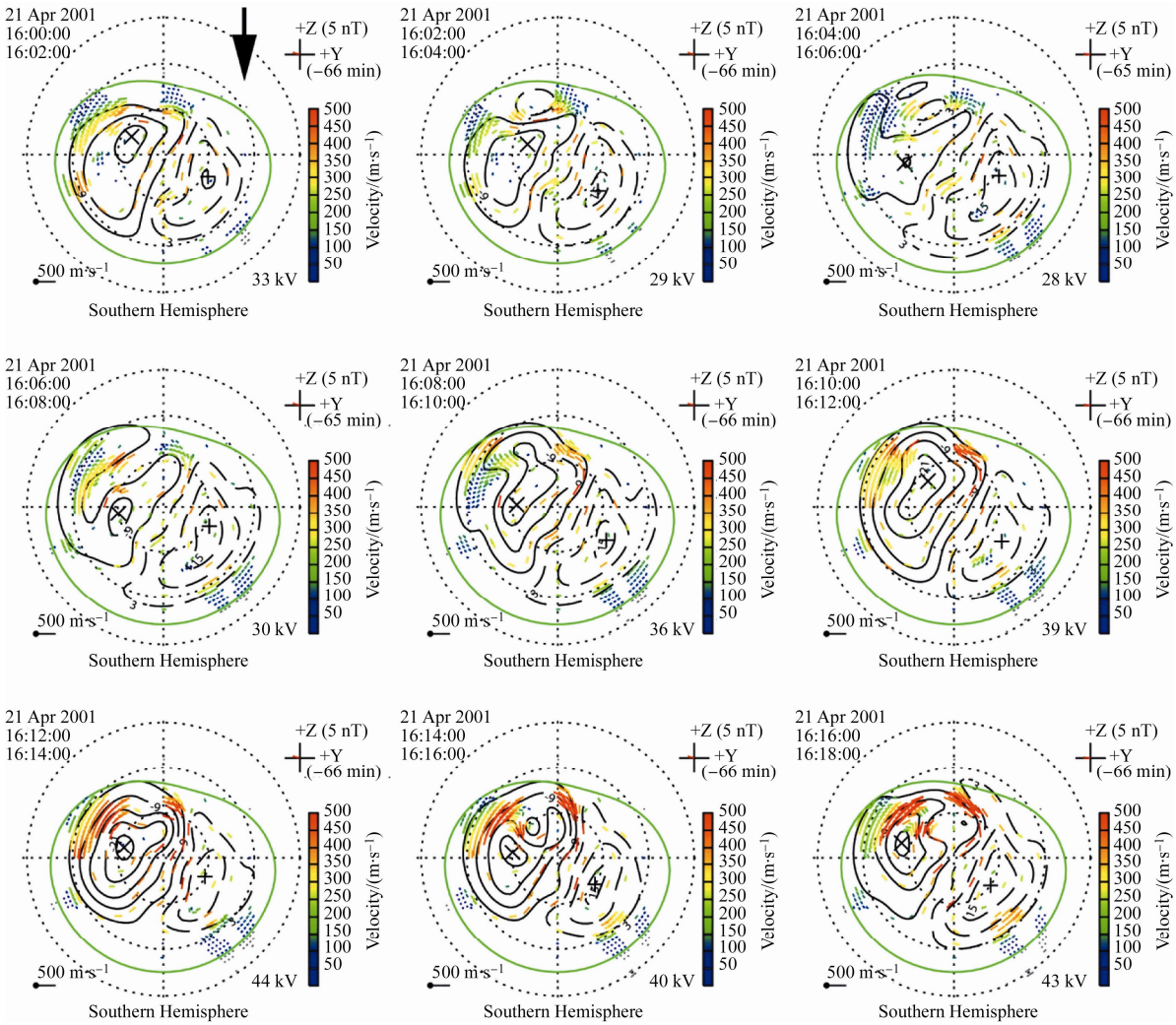

Figure 6 Two-dimensional plasma flow and electric potential derived from the Southern Hemisphere SuperDARN radars, fitted to a map potential model from 1600 to 1618 UT in 2-min intervals (1200 MLT at the top and 0600 MLT at the right of each frame). Colored points indicate "true" velocity vectors, which are the combination of the observed ionospheric LOS velocities and the component perpendicular to the LOS derived from the ionospheric potential model. The SI onset is marked by the black arrow in the first frame.

provides convincing evidence for the formation of downward FAC over ZHS on the duskside during the PI stage of an SI[17,31]. Figure 5 shows that the plasma flow was sunward within the main twin-vortex convection cell before the SI onset. After the SI onset, the figure shows that the plasma flow over ZHS was reversed (starting from the near range of the radar at 1602 UT), and this reversal lasted for ~8 min. According to the SI model prediction, the downward FAC formed during the PI stage of the SI, and this FAC drove a counterclockwise ionospheric plasma convection vortex (seen from above the Southern Hemisphere), in accordance with our optical and SuperDARN radar observations. Large-scale ionospheric convection shown in Figure 6 provides strong evidence for the generation of downward FAC in the afternoon sector; there is a complicated convection pattern with a multi-vortex flow system during the PI stage. These observational results suggest that a downward FAC formed during the PI stage of the SI. This downward FAC suppressed auroral particle precipitation and caused the plasma flow reversal.

After 1608 UT, the SI was in the MI stage and Figure 4 shows that the corresponding aurora over ZHS presented a new thin discrete arc with increasing luminosity. It is known that discrete auroral arcs are locations of upward FACs with intense emissions resulting from a magnetic field-aligned potential drop (inverted-V)[32]. The simultaneous radar observations covering the FOV of ZHS show that the plasma flow returned to the sunward direction with a higher velocity, as seen in Figure 5. The SI model of Araki[2] suggests that the FACs and ionospheric currents of the MI stage are in the same structure but with opposite polarity to that in the PI stage. Furthermore, the model indicates that the FACs in the MI stage are generated by enhanced magnetospheric convection under the shock compression of the magnetosphere and their magnitude should be much larger than that in the PI stage. Therefore, the optical auroral and radar observations as presented in Figures 4 and 5 are consistent with the model prediction.

One interesting observational signature of the ionospheric plasma flow in response to the IP shock compression is the clear periodical oscillation of the LOS velocity (namely repeated flow reversal) as shown in Figure 5. There is also westward phase propagation (backscatter echoes away from the radar) of the backscatter after the SI onset. To our knowledge, this shock-associated ionospheric convection phenomenon has not been reported in previous studies. Sato et al.[33] reported that a geomagnetic negative SI triggered one-to-one correspondence between quasi-periodic luminosity pulsations of a discrete aurora over ZHS and geomagnetic pulsations in the conjugate hemisphere. Because of the characteristic features, they advised that the phenomenon had a close relationship with the FLR caused by the sudden expansion of the magnetospheric cavity. Accordingly, we checked both the auroral sequence frames and keogram (not shown) in detail, but unfortunately did not find a clear periodically reforming auroral arc or pulsations during the SI.

The stack plots in Figure 7 show variations in the north-south component of the ground magnetic fields simultaneously recorded by the IMAGE magnetometer network in the Northern Hemisphere, whose geographical and geomagnetic information is given in Table 1. This network is aligned near the geomagnetic meridian where ZHS is located, and the nominal geomagnetically conjugate region of ZHS is located between HOR and LYR. In the stack plot, each color corresponds to a station and the lower eight curves show the raw waveforms whereas the upper eight curves are the band-pass filtered waveforms with a period range of 4–10 min for the clarification on variations associated with the oscillations of the plasma flow observed by the SENSU radar. A negative excursion of the X component was observed at the auroral zone observatories (MUO, PEL) immediately after the SI onset as marked by the vertical dashed line in Figure 7. This timing of the first negative pulsation is the same as that at the Jicamarca geomagnetic dip equator observatory, as shown in Figure 2. Such signatures are consistent with the SI model in the afternoon auroral zone[2]. As seen in Figure 7, the variation in the band-pass filtered magnetic field data at BJN (blue coded) was very similar to the oscillations of the plasma flow observed by SENSU radar and shown in Figure 5. The geomagnetic latitude of BJN is about 71.45°, about 3° latitude lower than that of the geomagnetically conjugated point of ZHS. These observations imply that there is a close relationship between the oscillations of the plasma flow and the magnetic pulsations.

The first cycle of the magnetic pulsation appeared at almost all observatories, and the pulsation amplitude peaked at HOR and BJN around 1606 UT. A distinct phase lag was observed between BJN and NAL, and there was a similar small phase lag between NUR and MUO. It is known that the FLRs oscillate in toroidal mode, which is observed as a characteristic amplitude peak at the resonance center and a 180° phase change as a function of latitude across the resonant peak[34-35]. Observations made by both the magnetometers and HF radars and the simulation results indicate that a pulse of solar wind dynamic pressure imposing on the magnetopause could drive FLRs with discrete frequencies at different latitudes where the field-line eigen frequencies match the frequency of the magnetospheric cavity modes[7,33,36-37]. Mann and Wright[38] showed that the magnetospheric flanks were a more fertile region of FLRs owing to larger velocity shear at the boundary between the streaming solar wind and magnetopause. Additionally, Rae et al.[39] presented an interval of extremely long-lasting narrow-band Pc5 pulsations during the recovery phase of a large geomagnetic storm. They found that SuperDARN HF radar observed clear oscillations of plasma flow in the duskside ionosphere with characteristic signatures of the FLRs. Thus, in view of these previous works on FLRs, magnetic observational results and simultaneous SuperDARN HF radar measurements of the present shock aurora event demonstrate a FLR characteristic feature caused by IP shock compression.

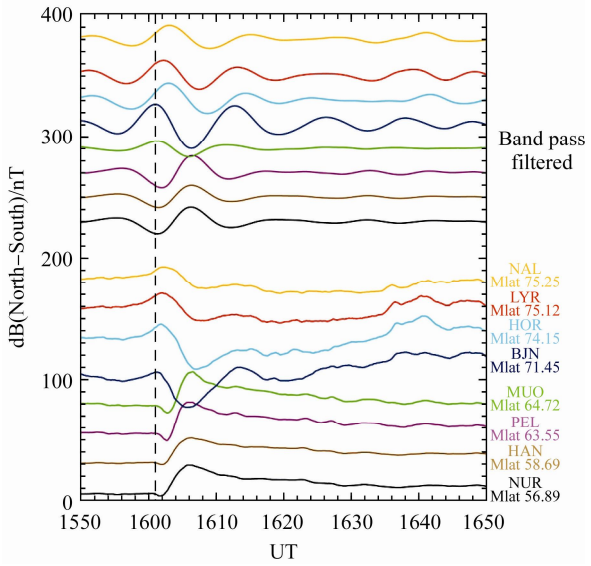

Figure 7 The lower eight curves of different color are raw waveforms for the north−south component recorded by IMAGE magnetometers in the Northern Hemisphere. The upper eight curves are the band-pass filtered data with a period range of 4–10 min.

ULF waves due to FLR activity play an important role in the transfer of energy from solar wind into the magnetospheric cavity and ultimately into the ionosphere[39]. The enhanced solar wind dynamic pressure carried by the IP shock imposed on the magnetopause and compressed the magnetosphere. This process induces compressional waves propagating in fast mode in the magnetosphere. Thus, a FLR will be excited where the eigen frequency of the field line matches the frequency of the fast wave[7].

4 Conclusion

Employing a favorable conjunction of an optical aurora

imager and simultaneous SuperDARN HF radar, we examined a shock aurora event on the duskside in the Southern Hemisphere. Results of this study are summarized as follows.

(1) During the PI stage of the SI triggered by IP shock sudden compression on the magnetosphere, the optical imager at ZHS did not observe aurora but with a distinct ionospheric plasma flow reversal and complicated convection pattern. We suggest that a downward FAC that formed immediately after the SI onset in the postnoon sector was responsible for these observational results.

(2) A new thin discrete auroral arc expanding westward over ZHS coincided with the MI stage of the SI, which may be associated with a field-aligned acceleration process in the region of the MI-related upward FACs. The lifetime of this discrete shock aurora was about 14 min.

(3) The major finding for the duskside shock aurora in this case study is the periodical oscillation of the plasma flow measured by the SuperDARN HF radar. Joint observations from the conjugated magnetometers indicate that this oscillation was associated with the FLR activity triggered by the sudden enhancement of the solar wind dynamic pressure.

Acknowledgements Geomagnetic data were kindly provided by IMAGE, WDC at Kyoto, and UCLA Ground Magnetometer Data Center. The IMF and solar wind data observed by ACE were obtained from CDAWed. This work was supported by the Polar Strategic Research Foundation of China (Grant no. 20100203), the National Natural Science Foundation of China (Grant nos. 40974083, 41031064, 40904041), the Ocean Public Welfare Scientific Research Project of China (Grant no. 201005017), the International Collaboration Supporting Project, Chinese Arctic and Antarctic Administration (Grant no. IC201303), and the National Basic Research Program of China (Grant no. 2010CB950503-06). Data were issued by the Data-sharing Platform of Polar Science (http://www.chinare.org.cn) maintained by Polar Research Institute of China and Chinese National Antarctic & Arctic Data Center.

References

1 Han D S, Yang H G, Liang J, et al. High-latitude reconnection effect observed at the dayside dip equator as a precursor of a sudden impulse. Journal of Geophysical Research, 2010, 115, A08214, doi:10.1029/2009JA014787.

2 Araki T. A physical model of the geomagnetic sudden commencement. in solar wind sources of magnetospheric ultra-low-frequency waves. Geophysical Monograph Series, 1994, 81: 183-200.

3 Han D S, Araki T, Yang H G, et al. Comparative study of Geomagnetic Sudden Commencement (SC) between Oersted and ground observations at different local times. Journal of Geophysical Research, 2007, 112, A05226, doi:10.1029/2006JA011953.

4 Yue C, Zong Q G, Zhang H, et al. Geomagnetic activity triggered by interplanetary shocks. Journal of Geophysical Research, 2010, 115, A00I05, doi:10.1029/2010JA015356.

5 Li X, Baker D N, Elkington S, et al. Energetic particle injections in the inner magnetosphere as a response to an interplanetary shock. Journal of Atmospheric and Solar-Terrestrial Physics, 2003, 65: 233-244.

6 Zhang X Y, Zong Q G, Wang Y F, et al. ULF waves excited by negative/positive solar wind dynamic pressure impulses at geosynchronous orbit. Journal of Geophysical Research, 2010, 115, A10221, doi:10.1029/2009JA015016.

7 Baddeley L J, Yeoman T K, McWilliams K A, et al. Global Pc5 wave activity observed using SuperDARN radars and ground magnetometers during an extended period of northward IMF. Planetary and Space Science, 2007, 55 (6): 792-808.

8 Laundal K M, Østgaard N. Persistent global proton aurora caused by high solar wind dynamic pressure. Journal of Geophysical Research, 2008, 113, A08231, doi:10.1029/2008JA013147.

9 Liou K, Newell P T, Shue J H, et al. "Compression aurora": Particle precipitation driven by long-duration solar wind ram pressure. Journal of Geophysical Research, 2007, 112, A11216, doi:10.1029/2007JA012443.

10 Zhou X Y, Strangeway R J, Anderson P C, et al. Shock aurora: FAST and DMSP observations. Journal of Geophysical Research, 2003, 108, A4, 8019, doi:10.1029/2002JA009701.

11 Zhou X Y, Tsurutani B T. Rapid intensification and propagation of the dayside aurora: Large scale interplanetary pressure pulses (fast shocks). Geophysical Research Letters, 1999, 26 (8): 1097-1100.

12 Motoba T, Kadokura A, Ebihara Y, et al. Simultaneous ground-satellite optical observations of postnoon shock aurora in the Southern Hemisphere. Journal of Geophysical Research, 2009, 114, A07209, doi:10.1029/2008JA014007.

13 Tsurutani B T, Lakhina G S, Verkhoglyadova O P, et al. A review of interplanetary discontinuities and their geomagnetic effects. Journal of Atmospheric and Solar-Terrestrial Physics, 2011, 73 (1): 5-19.

14 Boudouridis A, Zesta E, Lyons L R, et al. Effect of solar wind pressure pulses on the size and strength of the auroral oval. Journal of Geophysical Research, 2003, 108 (A4): 8012, doi: 10.1029/2002JA009373.

15 Boudouridis A, Lyons L R, Zesta E, et al. Nightside flow enhancement associated with solar wind dynamic pressure driven reconnection. Journal of Geophysical Research, 2008, 113, A12211, doi:10.1029/2008JA013489.

16 Boudouridis A, Lyons L R, Zesta E, et al. Dayside reconnection enhancement resulting from a solar wind dynamic pressure increase. Journal of Geophysical Research, 2007, 112, A06201, doi:10.1029/2006JA012141.

17 Liu J J, Hu H Q, Han D S, et al. Decrease of auroral intensity associated with reversal of plasma convection in response to an interplanetary shock as observed over Zhongshan Station in Antarctica. Journal of Geophysical Research, 2011, 116, A03210, doi:10.1029/2010JA016156.

18 Hori T, Shinbori A, Nishitani N, et al. Evolution of negative SI-induced ionospheric flows observed by SuperDARN King Salmon HF radar. Journal of Geophysical Research, 2012(in press).

19 Egeland A, Burke W J, Maynard N C, et al. Ground and satellite observations of postdawn aurorae near the time of a sudden storm commencement. Journal of Geophysical Research, 1994, 99 (A2): 2095-2108.

20 Sandholt P E, Farrugia C J, Burlaga L F, et al. Cusp/Cleft auroral activity in relationship to solar wind dynamic pressure, interplanetary magnetic field Bz and By. Journal of Geophysical Research, 1994, 99 (A9): 17323-17342.

21 Zhou X Y, Fukui K, Carlson H C, et al. Shock aurora: Ground-based imager observations. Journal of Geophysical Research, 2009, 114, A12216, doi:10.1029/2009JA014186.

22 Iyemori T. Storm-time magnetospheric currents inferred from mid-latitude geomagnetic field variations. Journal of Geomagnetism and Geoelectricity, 1990, 42: 1249- 1265.

23 Yang H, Sato N, Makita K, et al. Synoptic observations of auroras along the postnoon oval: a survey with all-sky TV observations at Zhongshan, Antarctica. Journal of Atmospheric and Solar-Terrestrial Physics, 2000, 62 (9): 787-797.

24 Hu H Q, Liu R R, Wang J F, et al. Statistic characteristics of the aurora observed at Zhongshan station, Antarctica. Chinese Journal of Polar Research, 1999, 11: 8-18.

25 Lyons L R, Blanchard G T, Samson J C, et al. Coordinated observations

demonstrating external substorm triggering. Journal of Geophysical Research, 1997, 102 (A12): 27039-27051.

26 Chisham G, Lester M, Milan S E, et al. A decade of the Super Dual Auroral Radar Network (SuperDARN): Scientific achievements, new techniques and future directions. Surveys in Geophysics, 2007, 28 (1): 33-109.

27 Ruohoniemi J M, Baker K B. Large-scale imaging of high-latitude convection with Super Dual Auroral Radar Network HF radar observations. Journal of Geophysical Research, 1998, 91 (A9): 10063-10079.

28 Burch J L, Reiff P H, Sugiura M. Upward electron beams measured by DE-1: A primary source of dayside region-1 Birkeland currents. Geophysical Research Letters, 1983, 10 (8): 753-756.

29 Klumpar D M, Heikkila W J. Electrons in the ionospheric source cone: Evidence for runaway electrons as carriers of downward Birkeland currents. Geophysical Research Letters, 1982, 9 (8): 873-876.

30 Marklund G, Blomberg L, Fälthammar C G, et al. On intense diverging electric field associated with black aurora. Geophysical Research Letters, 1994, 21 (17): 1859-1862.

31 Bristow W A, Lummerzheim D. Determination of field-aligned currents using the Super Dual Auroral Radar Network and the UVI ultraviolet imager. Journal of Geophysical Research, 2001, 106 (A9): 18577-18587.

32 Frank L A, Ackerson K L. Local-time survey of plasma at low altitudes over the auroral zones. Journal of Geophysical Research, 1972, 77 (22): 4116.

33 Sato N, Murata Y, Yamagishi H, et al. Enhancement of optical aurora triggered by the solar wind negative pressure impulse (SI-). Geophysical Research Letters, 2001, 28 (1): 127-130.

34 Samson J C, Jacobs J A, Rostoker G. Latitude-dependent characteristics of long-period geomagnetic micropulsations. Journal of Geophysical Research, 1971, 76 (16): 3675.

35 Mathie R A, Mann I R, Menk F W, et al. Pc5 ULF pulsations associated with waveguide modes observed with the IMAGE magnetometer array. Journal of Geophysical Research, 1999, 104 (A4): 7025.

36 Rae I J, Mann I R, Murphy K R, et al. Ground-based magnetometer determination of in situ Pc4–5 ULF electric field wave spectra as a function of solar wind speed. Journal of Geophysical Research, 2012, 117, A04221, doi: 10.1029/2011JA017335.

37 Walker A D M. Excitation of field line resonances by MHD waves originating in the solar wind. Journal of Geophysical Research, 2002, 107(A12): 1481, doi:10.1029/2001JA009188.

38 Mann I R, Wright A N. Diagnosing the excitation mechanisms of Pc5 magnetospheric flank waveguide modes and FLRs. Geophysical Research Letters, 1999, 26 (16): 2609.

39 Rae I J, Donovan E F, Mann I R, et al. Evolution and characteristics of global Pc5 ULF waves during a high solar wind speed interval. Journal of Geophysical Research, 2005, 110, A12211, doi:10.1029/2005JA011007.